Article

# Enhanced Activity of Enzymes Encapsulated in Hydrophilic Metal–Organic Frameworks

Weibin Liang, Huoshu Xu, Francesco Carraro, Natasha K. Maddigan, Qiaowei Li, Stephen G. Bell, David M. Huang, Andrew Tarzia, Marcello B Solomon, Heinz Amenitsch, Lisa Vaccari, Christopher J. Sumby, Paolo Falcaro, and Christian J. Doonan

*J. Am. Chem. Soc.*, **Just Accepted Manuscript** • DOI: 10.1021/jacs.8b10302 • Publication Date (Web): 12 Jan 2019

# Enhanced Activity of Enzymes Encapsulated in Hydrophilic Metal–Organic Frameworks

Weibin Liang[†], Huoshu Xu[‡], Francesco Carraro[§], Natasha K. Maddigan[†], Qiaowei Li[‡], Stephen G. Bell[†], David M. Huang[†], Andrew Tarzia[†], Marcello B. Solomon[†], Heinz Amenitsch[∥], Lisa Vaccari[⊥], Christopher J. Sumby[*†], Paolo Falcaro[*§,†], Christian J. Doonan[*†]

[†] Department of Chemistry and the Centre for Advanced Nanomaterials, The University of Adelaide, Adelaide, South Australia 5005, Australia

[‡] Department of Chemistry, iChEM (Collaborative Innovation Center of Chemistry for Energy Materials), and Shanghai Key Laboratory of Molecular Catalysis and Innovative Materials, Fudan University, Shanghai 200433, P.R. China

[§] Institute of Physical and Theoretical Chemistry, Graz University of Technology, Stremayrgasse 9, Graz 8010, Austria

[∥] Institute of Inorganic Chemistry, Graz University of Technology, Graz, Austria

[⊥] Elettra-Sincrotrone Trieste S.C.p.A, S.S. 14 Km 163,5 in AREA Science Park, 34149, Basovizza, Trieste, Italy

**ABSTRACT:** Encapsulation of biomacromolecules in metal–organic frameworks (MOFs) can preserve biological functionality in harsh environments. Despite the success of this approach, termed biomimetic mineralization, limited consideration has been given to the chemistry of the MOF coating. Here we show that enzymes encapsulated within hydrophilic MAF-7 or ZIF-90 retain enzymatic activity upon encapsulation and when exposed to high temperatures, denaturing or proteolytic agents, and organic solvents, whereas hydrophobic ZIF-8 affords inactive catalase and negligible protection to urease.

## INTRODUCTION

Metal–organic frameworks (MOFs) are a class of materials that are synthesized via a modular approach from metal-based nodes and organic links.[1] Recently, it has been shown that biomacromolecules can induce the growth of MOFs in aqueous solution to afford a robust coating that offers protection from environments that are typically destructive, such as elevated temperatures and proteolytic enzymes.[2-7] This facile process, termed biomimetic mineralization,[3, 8] does not require a co-precipitant and has been extended to other biological moieties, for example viruses[9, 10] and cells.[11, 12] Analogous strategies have also been successfully employed to encapsulate and stabilise enzymes using silica-based materials (biosilification).[13, 14] To date, zeolitic imidazolate framework-8 (ZIF-8), an extended network composed of $Zn^{2+}$ nodes and 2-methyl imidazole (HmIM) links,[15] is the most widely explored MOF for biomimetic mineralization.[7, 12] This is presumably because it can be synthesized under biologically compatible conditions.[12] However, an important aspect of ZIF-8 chemistry that has not been canvassed with respect to its suitability for biomineralization is its hydrophobicity.[16]

A significant body of research has focused on understanding how the structure and activity of proteins are modified by adsorption on surfaces.[17] The adsorption process is intrinsically complex; however, it is known that proteins tend to have a greater affinity for hydrophobic surfaces[17] and that hydrophobic interactions often engender conformational changes that denature the protein and lead to loss of activity.[18] Indeed, we have observed that particular enzymes, e.g. catalase, are inactive when encapsulated within ZIF-8 crystals (vide infra). Thus, we were motivated to examine whether more hydrophilic ZIF materials would be more compatible with enzymes and lead to retention of catalytic activity. ZIF-8,[6] ZIF-90,[19] and MAF-7[16] are all Zn-based ZIFs of sodalite topology that possess analogous structure metrics; however, their chemically distinct organic links significantly modify the hydrophobicity/philicity of their respective frameworks (Figure S1). For example, water adsorption isotherms confirm that MAF-7 (links: 3-methyl-1,2,4-triazolate, MTZ) and ZIF-90 (links: 2-imidazolate carboxaldehyde, ICA) are dramatically more hydrophilic than ZIF-8.[16, 20] Here we encapsulate catalase and urease and compare the activities of biomolecules within ZIF-8, ZIF-90, and MAF-7. Our data show that the activity of both enzymes is significantly

enhanced in MAF-7 and that the enzymes show negligible (urease) or no activity (catalase) within ZIF-8.

## EXPERIMENTAL SECTION

### Syntheses

All chemicals and solvents were purchased from commercial sources and used as received without further purification.

### Fluorescein-tagged enzyme

Fluorescein isothiocyanate (FITC, 0.5 mg) and catalase (CAT; Sigma-Aldrich, catalase from bovine liver, 2000-5000 units $mg^{-1}$ protein, 40 mg) was dissolved in carbonate-bicarbonate aqueous buffer solution (0.1 M, pH 9.2, 4 mL) and left for two hours in darkness at room temperature under gentle stirring. The FITC-tagged CAT (FCAT) was recovered by passing the reaction mixture through an Illustra NAP-25 column (GE Healthcare Life Sciences, NSW, Australia). The crude FCAT solution was concentrated through a 10 K membrane by centrifugation at 4°C (4,000 rpm for 20 min), followed by solvent-exchange with ultrapure water. The concentration-solvent-exchange process was repeated two times to ensure the buffer salts were completely removed from the solution. Thereafter, the concentrated FCAT aqueous solution was passed through an NAP-25 column again to ensure the completely removal of unreacted FITC. The obtained FCAT solution was stored in darkness at 4°C.

A similar method was used to prepare fluorescein-tagged peroxidase from horseradish (FHRP; Sigma-Aldrich, Tye VI-A, lyophilized powder, 950-2000 units $mg^{-1}$ solid (using ABTS), $\geqslant$ 250 units $mg^{-1}$ (using pyrogallol)) and fluorescein-tagged urease from *Canavalia ensiformis* (Jack bean) (Furease; Sigma-Aldrich, Type III, powder, 15000-5000 units $g^{-1}$ solid).

### Synthesis method for FCAT@ZIF-8

FCAT@ZIF-8 was synthesized in water with $Zn(OAc)_2 \cdot 2H_2O$ (40 mM), 2-methylimidazole (HmIM, 640 mM) and FCAT (0.33 mg $mL^{-1}$ ) at room temperature under static condition (without stirring) for 24 h. The precipitate was recovered by centrifugation at 10,000 r.p.m. for 5 min and then washed, sonicated, and centrifuged three times each in ultrapure water to remove loosely adsorbed FCAT.

### Synthesis method for FCAT@ZIF-90

FCAT@ZIF-90 was synthesized in water with $Zn(NO_3)_2 \cdot 6H_2O$ (40 mM), 2-imidazolecarboxaldehyde (HICA, dissolved at elevated temperature; 160 mM) and FCAT (0.33 mg $mL^{-1}$) at room temperature under static condition for 24 h. The precipitate was recovered by centrifugation at 10,000 r.p.m. for 5 min and then washed, sonicated, and centrifuged three times each in ultrapure water to remove loosely adsorbed FCAT.

### Synthesis method for FCAT@MAF-7

FCAT@MAF-7 was synthesized in water with $Zn(NO_3)_2 \cdot 6H_2O$ (40 mM), 3-methyl-1,2,4-triazole (Hmtz, 120 mM), 10% $NH_3 \cdot H_2O$ (60 µL) and FCAT (0.33 mg $mL^{-1}$) at room temperature under stirring for 24 h. The precipitate was recovered by centrifugation at 10,000 r.p.m. for 5 min and then washed, sonicated, and centrifuged three times each in ultrapure water to remove loosely adsorbed FCAT.

### Characterization

### Powder X-ray diffraction (PXRD)

PXRD patterns were obtained using a D4 ENDEAVOR X-ray Diffractometer from Bruker. A Co anode was used to produce $K_\alpha$ radiation ($\lambda$ = 1.78897 Å). Flat plate diffraction data was collected from the range $2\theta$ = 5–40 °. The PXRD data were modified by PowDLL Converter (version 2.68.0.0) and expressed as the copper-source irradiated patterns ($\lambda$ = 1.54056 Å).

### Thermogravimetric analysis (TGA)

TGA data was collected on a Simultaneous Thermal Analysis–STA (TGA/DSC) from LINSEIS THERMAL ANALYSIS. Approximately 5 mg of sample was placed on a ceramic pan and heated from 30 to 800 °C at a rate of 5 °C $min^{-1}$. Each sample was heated under a constant flow of *ca.* 30 L $min^{-1}$ air.

### Fourier transform infrared (FTIR) spectroscopy

FTIR spectra of ZIFs and biomacromolecule/ZIF composites were obtained on a Perkin Elmer Spectrum 100 FT-IR Spectrometer using approximately 0.5 mg of ground sample. Sixteen scans were recorded over the range of 40000-650 $cm^{-1}$

### Gas sorption

Gas adsorption isotherms were obtained on a Micromeritics 3Flex Surface Characterisation Analyser. Approximately 20 mg of sample was placed into a glass analysis tube and degassed under dynamic vacuum for 12 h at 105 °C prior to measurement. Nitrogen ($N_2$) adsorption and desorption isotherms were measured at 77 K. The isotherms were then analyzed to determine the Brunauer-Emmet-Teller (BET) surface area using the MicroActive software (Version 3.00, Micromeritics Instrument Corp. 2013).

### Confocal laser scanning microscopy (CLSM)

The presence and spatial location of the fluorophore-tagged biomolecules in (or on) the MOF composites was determined using CLSM technique (Olympus FV3000 Confocal Laser Scanning Microscope, OLYMPUS). The fluorescein-tagged biomolecules were excited at 488 nm and the fluorescence signal was collected in a window from 495 to 545 nm.

### Fluorescence spectrophotometry

Fluorescence measurements of solution samples were carried out using a Varian Cary Eclipse or a HITACHI F-7000 Fluorescence Spectrophotometer.

### Scanning electron microscopy (SEM)

SEM images were collected using a Philips XL30 Field Emission Scanning Electron Microscope (FESEM). Prior to analysis, the samples were dispersed in ethanol by

sonication, drop-cast on a 12 mm aluminum SEM stage, and sputter-coated with a 10 nm platinum thin film.

**Synchrotron attenuated total reflection fourier-transform infrared spectroscopy (ATR-FTIR) analysis**

The following samples have been measured by ATR-FTIR analysis: CAT, MAF-7, CAT-on-MAF-7, CAT@MAF-7, ZIF-8, CAT-on-ZIF-8, CAT@ ZIF-8, ZIF-90, CAT-on-ZIF-90, CAT@ZIF-90. Measurements have been done at Chemical and Life Sciences branch of SISSI beamline at Elettra-Sincrotrone Trieste, using the vertex 70 interferometer (Bruker GmBH), equipped the conventional Globar MIR source and DTGS detector. A single reflection ATR accessory (MIRacle, PIKE Technologies) with diamond Infrared Reflection Element (IRE) has been used. Samples have been transferred on to the crystal by using a micropipette or a needle, depending on their texture. Repeated spectra have been collected in the 4000-700 $cm^{-1}$ spectral range averaging 128 scans at 4 $cm^{-1}$ spectral resolution with a scanner velocity of 5 KHz upon complete sample dehydration. A final spectrum has been then acquired averaging 512 scans at the same conditions. Fourier transform was carried out with Mertz phase correction, Blackman-Harris 3-terms apodization function. Spectra were rationed against a background acquired onto the clean IRE. Second derivatives have been computed with the Savitzky–Golay algorithm with 13 smoothing points. For comparison purposes, second derivative spectra have been vector normalized in the 1800-1480 $cm^{-1}$ spectral region.

**Catalytic performance of FCAT and FCAT/MOF composites**

The Ferrous Oxidation in Xylenol orange (FOX) assay was applied to quantify the $H_2O_2$ concentration.[21] FCAT or FCAT/MOF composite was added into stirred Tris-HCl buffer (50 mM, pH 8, 500 μL). Thereafter, various amounts of $H_2O_2$ stock solution (5 mM in water) was added. The volume of the reaction mixture was adjusted to 1 mL by water. The catalyst concentration (based on FCAT) in the enzymatic reaction was 20 nM. At different time intervals, 50 μL aliquots of the mixtures were sampled and mixed with 950 μL FOX reagent in an eppendorf tube and then incubated at least 30 min at room temperature. After incubation, the samples were centrifuged. The UV–visible absorbance at 585 nm for the supernatant were recorded to calculate the $H_2O_2$ concentration. The reaction rate ($V_{obs}$, mM $s^{-1}$) is defined as the initial $H_2O_2$ decomposition velocity of the enzymatic assay.

**RESULTS AND DISCUSSION**

Catalase (CAT) is an iron-heme enzyme that catalyzes the decomposition of hydrogen peroxide to water and oxygen.[22] In this study we employed fluorescein-tagged CAT (FCAT) to determine the spatial distribution and enzyme loading within the ZIF-based biocomposites. The synthesis of ZIF-8 or ZIF-90 in the presence of FCAT was performed using established protocols to yield FCAT@ZIF-8 or FCAT@ZIF-90, respectively.[6] The synthetic approach for MAF-7-coated FCAT (FCAT@MAF-7) was analogous to that of FCAT@ZIF-8; however, $Zn(NO_3)_2 \cdot 6H_2O$ was used as the metal source and dilute ammonium hydroxide solution was employed as a base.[16] To compare the activities of encapsulated and surface-adsorbed FCAT, we also synthesized biocomposites by mixing FCAT with pure ZIF-8, ZIF-90, or MAF-7 crystals in water at room temperature (RT) for 4 hours. Rigorous washing procedures (e.g. 10% w/w aq sodium dodecyl sulfate (SDS)) could not effectively remove the surface-adsorbed FCAT-on-ZIF-90 and FCAT-on-MAF-7 (Figures S2-S4), and thus, to be consistent, all as-synthesized biocomposites were only washed with water to remove the loosely adsorbed FCAT on the ZIF surface. The prepared biocomposites are illustrated in Figure 1a. In addition, in order to elucidate the formation mechanism of the CAT/MOF biocomposities, synchrotron X-ray diffraction experiments (stop-flow set-up) were conducted to examine the MOF formation in the presence or absence of CAT. Experimental results reveal that CAT@ZIF-8 is formed through the biomineralization process (Figure S5), however, CAT@MAF-7 and CAT@ZIF-90 are formed through the co-precipitation mechanism (Figure S5).

Samples of the as-synthesized biocomposites were examined by PXRD, which confirmed that they were phase pure and possessed the sodalite topology (Figure S6). The crystal size and morphology were assessed by SEM, which showed that FCAT@ZIF-8 and FCAT@ZIF-90 samples were dispersed rhombododecahedral crystals whereas some crystal intergrowth was observed for FCAT@MAF-7 (Figure S7). Gas adsorption isotherms were conducted to assess porosity, yielding Brunauer-Emmett-Teller (BET) surface areas of 1205.7(21.2), 1059.2(2.0), and 1070.6(2.2) $m^2$ $g^{-1}$ for FCAT@ZIF-8, FCAT@ZIF-90, and FCAT@MAF-7, respectively (Figures S8–S10). Furthermore, comparison of the pore size distributions of the biocomposites and their corresponding neat ZIFs suggests that enzyme encapsulation does not affect the bulk pore structure of the ZIFs (Figures S8–S10). The spatial distribution of FCAT within the samples was assessed using confocal laser microscopy (CLSM) (Figure 1b and S12); the images show that the FCAT molecules were more homogeneously distributed throughout FCAT@MAF-7 and FCAT@ZIF-90 crystals than in FCAT@ZIF-8, in which FCAT was predominantly located in the sub-surface region. The latter data is in agreement with our previous studies,[6] and shows that the hydrophilic and hydrophobic ZIFs give rise to different enzyme spatial distributions. FCAT loading in all samples was determined by tracing its fluorescence signal after dissolution in 0.1 M citric acid-sodium citrate buffer (pH 5) (Table S1). The weight percentage of enzyme encapsulated varied from 0.5 to 3.3 wt% for FCAT-on-MAF-7 to FCAT@ZIF-8, respectively (Figure 1b and Table S1). It is noteworthy that higher FCAT loading in the biocomposites can be achieved by using higher dosage of FCAT in the synthesis (Table S1).

To determine the effect of framework chemistry on the performance of the encapsulated enzyme, we measured $H_2O_2$ decomposition for each of the FCAT/ZIF composites. For comparison, we also evaluated the activity of free FCAT under the same conditions. In addition, we have found that the handling conditions for the ZIF-based biocomposites can affect the integrity of the ZIF coating. For example, phosphate buffers, such as PBS, give rise to rapid decomposition of ZIF-8 crystals and we anticipate that this will affect enzyme activity studies. As a consequence, we avoided exposing our biocomposites to PBS. Ongoing work in our laboratory is focused on establishing protocols for the storage, handling and activity studies of ZIF-based biocomposites. A noteworthy result, shown in Figure 1c, Figures S22–S26 and Table S2, is that FCAT@ZIF-8 composites showed no measurable catalytic activity. (Figure 1a and 1c). Furthermore, FCAT adsorbed onto the surface of ZIF-8 was also inactive (Figure 1a and 1c). We believe that the slightly slower reaction rates of FCAT-on-MAF-7 and FCAT-on-ZIF-90 compared to FCAT@MAF-7 and FCAT@ZIF-90 may be attributed to hindered substrate diffusion and/or changed enzyme orientation that is engendered by closed packing of FCAT on the MOF surface (surface crowding effect).[23-26] Similar phenomenon was observed in the case of fluorescence-tagged horseradish peroxidase (FHRP, Figure S39). These data are consistent with studies that show protein adsorption on hydrophobic surfaces can lead to a loss of activity[17, 18] and suggests recent reports of enzyme activity for FCAT@ZIF-8 may need to be re-evaluated.[27-29] In contrast to the FCAT/ZIF-8 biocomposites, FCAT@MAF-7 showed comparable activity to that of free FCAT: $3.2 \times 10^{-3}$ mM $s^{-1}$ for FCAT@MAF-7 versus $4.4 \times 10^{-3}$ mM $s^{-1}$ for free FCAT (Figure 1c, S24 and S25). Additionally, FCAT@ZIF-90 showed a substantial reduction in activity compared with the free enzyme ($1.4 \times 10^{-3}$ mM $s^{-1}$, Figure 1c and S26). To provide a more comprehensive comparison of the FCAT/MOF biocomposite with free FCAT we evaluated the Michaelis-Menten kinetic parameters (Figure S28 and Table S2). The $K_m$ and $k_{cat}$ values for FCAT@MAF-7 are 0.99 mM and 950 $s^{-1}$, respectively (Table S2), which are comparable to free FCAT and superior to FCAT@ZIF-90 (Figure S28 and Table S2). The loss of activity for the FCAT/ZIF-8 biocomposites could be due to a number of factors, such as 1) the presence of the acetate anion inhibiting the FCAT activity; 2) binding of HmIM to the iron-heme active site of FCAT during the synthesis process; 3) denaturation of the enzyme during the encapsulation or surface immobilization process as a result of hydrophobic interactions between FCAT and ZIF-8; and/or 4) hindered diffusion of the substrate ($H_2O_2$)/product ($H_2O$) by the hydrophobic framework of ZIF-8 (for FCAT@ZIF-8). Importantly, CAT (i.e. not fluorescein tagged) was found to be inactive for the CAT@ZIF-8 composites (Figure S28), indicating the deactivation of FCAT in/on ZIF-8 is not ascribed to the enzyme surface functionalization.

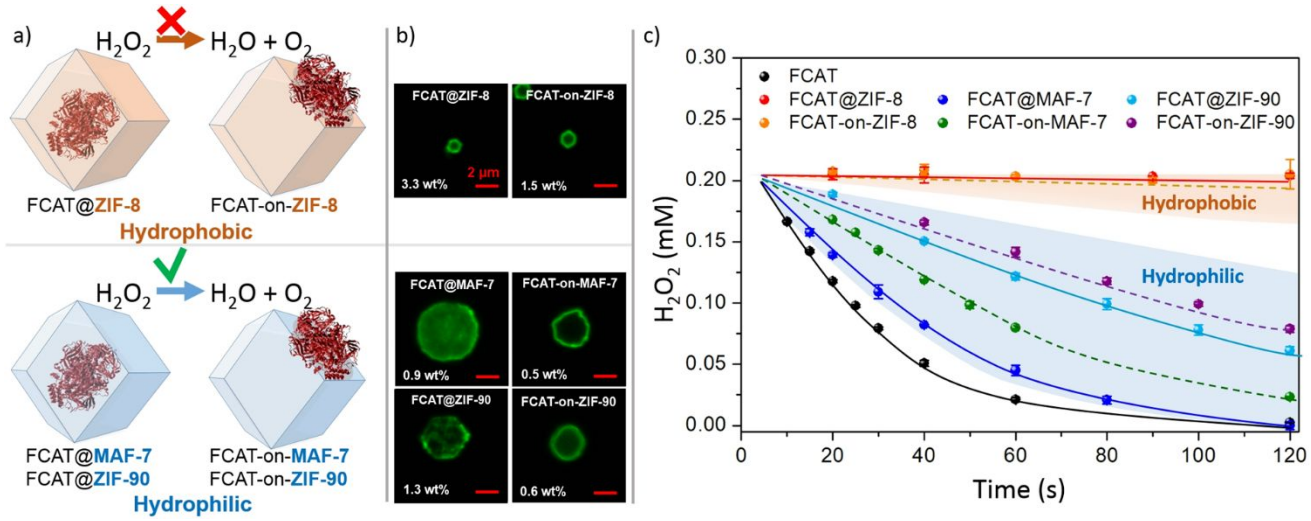


Figure 1. (a) Schematic representations of the different FCAT/ZIF biocomposites formed by encapsulation of enzyme molecules via biomimetic mineralization or surface adsorption within/on hydrophobic (orange) or hydrophilic (blue) frameworks. (b) Confocal laser scanning micrographs showing fluorescence of different FCAT/ZIF biocomposites. (c) Catalytic activity of FCAT and different FCAT/ZIF composites. The assay was performed with FCAT concentration of 20 nM and $H_2O_2$ concentration of 0.20 mM.

High concentrations of acetate anions (>0.3M) have been reported to progressively inhibit the enzymatic activity of catalase.[30] In order to eliminate that the deactivation of FCAT in/on FCAT@ZIF-8 is derived from the presence of acetate anion during synthesis we examined the catalytic activity of FCAT after incubating the catalyst in 40 mM Zn(OAc)2·2H2O or NaOAc at room temperature for two hours. Enzymatic assay data demonstrated that acetate ion concentration (40 mM) did not inhibit FCAT activity (Figure S21). We note that even under synthesis conditions the acetate concentration is less than the inhibitory amount, and further the

postsynthetic washing procedure eliminates residual acetate that may be present on the biocomposites. Thus, we conclude that the deactivation mechanism for FCAT in or on ZIF-8 is not due to the presence of acetate anions in the synthesis or residual acetate in the biocomposite sample. To further elucidate the deactivation mechanism we synthesized the biocomposites CAT@ZIF-8, CAT@MAF-7, CAT-on-ZIF-8, and CAT-on-MAF-7 in the absence of a fluorescein tag for spectroscopic examination. Figure 2a shows the UV–visible spectra of the ZIF-based biocomposites compared with free CAT. The Soret absorption band at 407 nm ($\pi$-$\pi^*$), due to the iron-heme cofactor in CAT, does not shift position in the solid-state UV–visible spectra of CAT@ZIF-8 and CAT@MAF-7 (Figure 2a). Moreover, we carried out a control experiment that showed the enzymatic activity of FCAT is not affected by the presence of HmIM (Figure S20). These data suggest that the heme-binding pocket is not modified in the biocomposites and provides evidence that the HmIM does not inhibit the active site of the enzyme.[31] To obtain information about changes to the tertiary structure of CAT, we examined the CAT/ZIF biocomposites using fluorescence spectroscopy. Owing to absorption of the ICA ligand overlapping with the fluorescence signal of tryptophan at ~334 nm, CAT/ZIF-90 samples could not be analysed. The tryptophan-derived (Trp-14, -142, -182, -185, -276, and -302) fluorescence emission profile of CAT is sensitive to the environment,[22] i.e. whether they are buried in the interior of the enzyme or exposed to solvent.[32] CAT@MAF-7, CAT-on-MAF-7, and CAT@ZIF-8 show essentially identical emission profiles to free CAT; however, $\lambda_{max}$ for CAT on ZIF-8 is blue-shifted to 330 nm (versus 335 nm for free CAT, Figure 2b). These data suggest that the tertiary structure of CAT is perturbed upon immobilization on the ZIF-8 crystal surface and may explain why the adsorbed enzyme is catalytically inactive (Figure 1c). Finally, the lack of an observable shift in $\lambda_{max}$ for FCAT@ZIF-8 suggests that hindered diffusion of the substrate ($H_2O_2$)/product ($H_2O$) by the hydrophobic framework of ZIF-8 (point 4, vide supra) may play a role.

Further insight into the structure of the encapsulated and surface adsorbed CAT was achieved through FTIR experiments. The FTIR spectrum of pure catalase is shown in Figure 3**, S131, and S14**. The characteristic normal modes of vibration of the peptide backbone are the amide I (1700-1610 cm$^{-1}$) and amide II (1595-1480 cm$^{-1}$) bands.[33, 34] The amide I vibration is mainly comprised of the C=O stretching vibration (~80%), with minor contributions from the out-of-phase CN stretching vibration, the CCN deformation, and the NH in-plane bend. The amide I band is the most intense feature in the FTIR spectrum, and therefore, is commonly used to assess the secondary structure of a given protein.[34] The amide I band of dehydrated CAT shows three major spectral contributions (1683, 1654 and 1635 cm$^{-1}$) (Figure 3 and S13) that are more clearly observed in the second derivative spectrum in Figure S3b, 3d, 3f, and S13. The spectral component centered at 1654 cm$^{-1}$ is assigned to alpha-helix motifs while the feature at 1635 cm$^{-1}$ can be attributed to intramolecular beta-sheets. The least intense feature at 1683 cm$^{-1}$ is engendered by protein turns and loops. The position of these peaks is dependent on the secondary structure of CAT, which is a tetramer composed of four subunits, that contains both alpha-helix and beta-sheet motifs in proportion 30% and 18% respectively (PDB ID 1A4E[35]). The amide II mode (1595-1480 cm$^{-1}$) is the out-of-phase combination of the N-H in plane bending (~60%) and the CN stretching (~40%) vibrations with smaller contributions from the CO in plane bend and the CC and NC stretching vibrations. Typically, the amide II band is less influenced by protein secondary structure with respect to the amide I band. In the case of CAT, the amide II band shows a major contribution at 1545 cm$^{-1}$, which is due to an alpha-helix motif. A second contribution centered at 1515 cm$^{-1}$ can be assigned to intramolecular beta-sheets and finally a minor contribution at 1579 cm$^{-1}$, associated to turns and loops.[33]

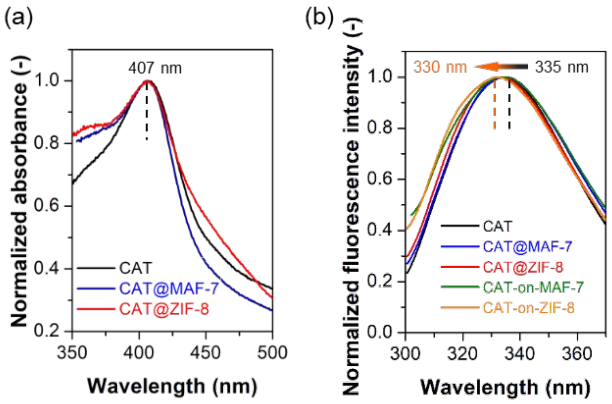


Figure 2. (a) Solid-state UV–visible spectra for catalase (CAT), CAT@MAF-7, and CAT@ZIF-8. (b) Fluorescence spectra of CAT and different FCAT/MOF composites. Measurements were carried out with CAT concentration of 1 µM in 0.1 M Tris-HCl buffer (pH 8).

Close inspection of Figure 3a confirms that CAT is either absorbed on or encapsulated in ZIF-8. This is evidenced by 1) the appearance of the amide I peak in the 1700-1600 cm$^{-1}$ spectral region and 2) the broadening at lower wavenumbers of the ZIF-8 peak centered at 1585 cm$^{-1}$, due to the overlap with the amide II band. Analysis of the second derivative spectra, shown in Figure 3b, indicates a significant shift in the spectral bands associated with protein compared to pure CAT. For encapsulated CAT, the peaks associated with the turns and loops (centered at 1683 cm$^{-1}$) and to the alpha-helix (centered at 1655 cm$^{-1}$, broadened at higher wavenumbers due to convolution with the 1666 cm$^{-1}$ band of ZIF-8) motifs are evident. However, the peak associated with the intermolecular beta-sheets is shifted ca. 8 cm$^{-1}$ (Figure 3b). This peak position is usually associated to intermolecular beta-sheet structure present in the protein aggregates.[36] For absorbed

CAT, the alpha-helix mode is not detectable, while a major spectral contribution centered at about 1638 $cm^{-1}$, and a minor shoulder at 1614 $cm^{-1}$ have appeared. The first spectral contribution (1638 $cm^{-1}$) can be attributed to intermolecular beta-sheets as the band shifts are smaller than the spectral resolution (set at 4 $cm^{-1}$) while the second to extended intermolecular aggregates.[37] Overall, the collected data support the hypothesis that the hydrophobic nature of ZIF-8 induces the aggregation of both encapsulated and absorbed CAT (Figure 3b).

From Figure 3c, the presence of CAT in the MOF, either absorbed or encapsulated in MAF-7, can be confirmed by the appearance of the amide I peak in the 1700-1600 $cm^{-1}$ spectral region and by the broadening at higher wavenumbers of the MAF-7 peak centered at 1491 $cm^{-1}$, due to spectral interference of the amide II band. Analysis of second derivative spectra (Figure 3d) shows that the position of the amide II peaks associated to CAT alpha helix and intermolecular beta-sheet secondary structures is essentially unchanged with respect to free CAT. Accordingly, the FTIR data suggests that the secondary protein structure is preserved when adsorbed on or encapsulated within hydrophilic MAF-7. The absorbance spectrum of ZIF-90 is shown in Figure 3e, has a prominent mode centered at 1671 $cm^{-1}$, extending from 1751 to 1551 $cm^{-1}$, that is attributed to a C=O stretch.[19] The position and intensity of this carbonyl band obscures the amide I and, partially, the amide II spectral features, (see Figure 3e and 3f). Figure S14 shows the amide II spectral region with two peaks centered at about 1540 and 1515 $cm^{-1}$. The position of these bands is consistent with the amide II components of free CAT. We note that these peaks are similar to those observed in the spectra of CAT-on-MAF-7. However, as shown in Figure 3d, only the higher frequency peak can be distinguished which is centered about 1543-1546 $cm^{-1}$ for the absorbed and encapsulated protein. In the case of CAT/ZIF-90, a significant blue shift of the amide II peak to about 1563 $cm^{-1}$ was observed. Despite the lower sensitivity of amide II to protein secondary structure with respect to amide I, we contend that the secondary structure of CAT on/@ ZIF-90 behaves comparably to CAT in/on MAF-7 (Figure 3e and 3f).

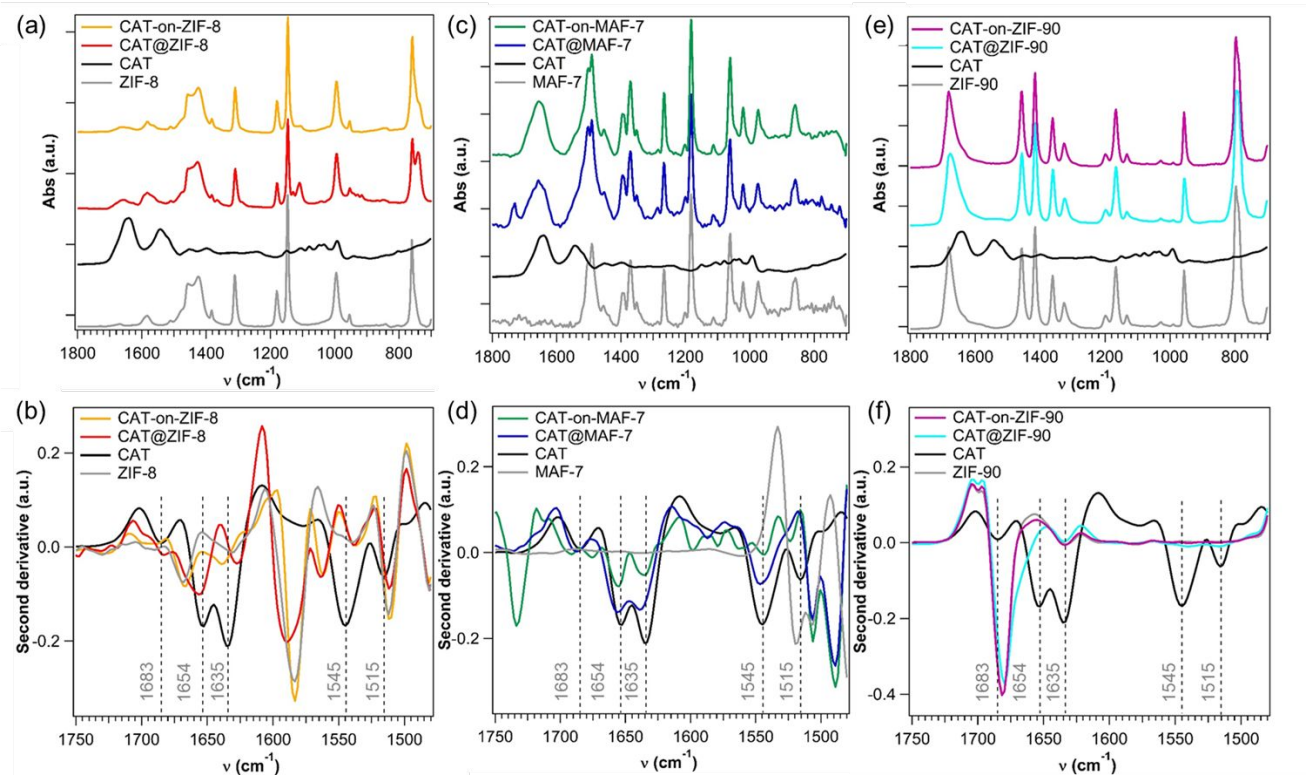


Figure 3. ATR-FTIR spectra (1800-750 $cm^{-1}$) and the corresponding second derivative ATR-FTIR spectra (vector normalized in the spectra region 1750-1480 $cm^{-1}$) of (a and b) ZIF-8 (gray), CAT (black), CAT@ZIF-8 (red) and CAT-on-ZIF-8 (orange); (c and d) MAF-7 (grey), CAT (black), CAT@MAF-7 (blue), and CAT-on-MAF-7 (green); and (e and f) ZIF-90 (grey), CAT (black), CAT@ZIF-90 (cyan), and CAT-on-ZIF-90 (purple). Grey dash lines in b, d, and f indicate the ATR-FTIR spectral vibrations of the amide I (1683, 1654, and 1635 $cm^{-1}$) and amide II (1545 and 1615 $cm^{-1}$) bands for CAT. The spectral component for amide I band centered at 1654, 1635, and 1683 $cm^{-1}$ are assigned to the alpha-helix motifs, intramolecular beta-sheets, and protein turns and loops in free CAT, respectively. The spectral component for amide II band centered at 1545 and 1615 $cm^{-1}$ are assigned to the alpha-helix motif and the intramolecular beta-sheets of CAT, respectively.

Given that the catalytic activity of the encapsulated enzymes is preserved for FCAT@MAF-7 and FCAT@ZIF-90 (Figure 1c), we sought to examine the capacity of these ZIF coatings to protect the enzymes from inhospitable environments. This 'shielding' effect has been previously observed for ZIF-90;[9] thus, it serves as an excellent benchmark material for FCAT@MAF-7. To assess the capacity of the ZIF coating to protect the biological cargo from elevated temperatures, we measured the enzymatic activity for FCAT, FCAT@MAF-7, and FCAT@ZIF-90 after incubating the catalysts at 50, 60, and 70 °C (Figure 4a and S29), along with a room temperature (RT, 25 ± 1 °C) control experiment. As anticipated, without protection via encapsulation the activity of free FCAT decreased dramatically from $3.7 \times 10^{-3}$ mM $s^{-1}$ at RT to $0.9 \times 10^{-3}$ mM $s^{-1}$ after treatment at 70 °C. Consistent with previous studies, ZIF-90 provides a degree of protection for embedded FCAT: *ca.* 80 and 65% of its original activity was retained after exposure to 50 and 60 °C, respectively. Notably, FCAT@MAF-7 offered far superior protection to elevated temperatures than ZIF-90, retaining 79% of its original activity after exposure to a temperature of 70 °C compared with 24% and 25% for FCAT and FCAT@ZIF-90, respectively. We then exposed the ZIF-based biocomposites to urea, a chaotropic agent that engenders loss of biological function by unfolding proteins.[38] Figure 4a shows that free FCAT retained only 8% of its original activity after contact with urea; however, FCAT@MAF-7 and FCAT@ZIF-90 maintained 89 and 48% of their original activity, respectively. It is worth noting that analogous experiments employing FCAT-on-MAF-7 and FCAT-on-ZIF-90 led to essentially complete deactivation of the surface-adsorbed protein (Figure S30). Thus, by exposing FCAT@MAF-7 and FCAT@ZIF-90 to urea we were only observing enzymatic activity from encapsulated enzyme. In the presence of protease (2 mg $mL^{-1}$ for 4 h at RT) FCAT@MAF-7 retained 85% of its original activity compared with only 14% for free FCAT and 19% for FCAT@ZIF-90 (Figure 4a and S31). Both MAF-7 and ZIF-90 possess Å-sized pore apertures that would size-exclude the protease and prevent contact with the embedded enzyme. FCAT@MAF-7 and FCAT@ZIF-90 retained 85 and 19% of their catalytic activity. This is commensurate with urea treatment and is again presumably due to the deactivation of the surface-adsorbed enzyme, which is more significant in the latter (Figure S31). Finally, both MAF-7 and ZIF-90 protect the embedded FCAT from organic solvents (Figure 4a). Specifically, FCAT@MAF-7 maintained 96 and 64% of its original activity after exposure to dimethyl sulfoxide (DMSO) and tetrahydrofuran (THF), respectively. In comparison, the activity of free FCAT is significantly diminished upon exposure to these solvents (Figure 4a). These experiments suggest that MAF-7 offers superior protection to enzymes than other reported ZIFs and may provide the stability necessary for the enzymes to retain their performance under commercially relevant conditions.[39]

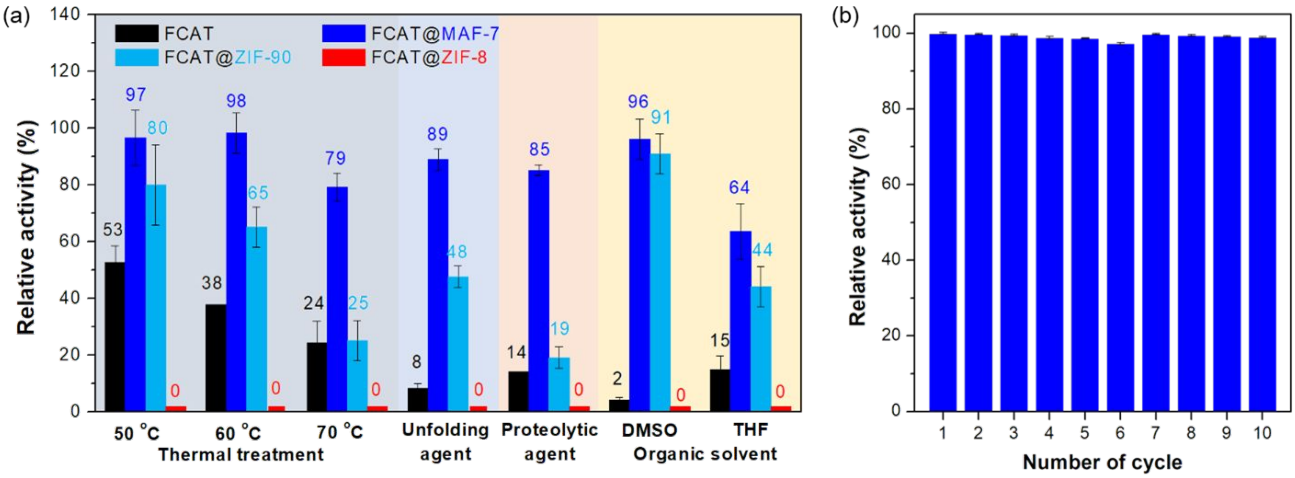


Figure 4. (a) Activity of FCAT, FCAT@MAF-7, FCAT@ZIF-90, and FCAT@ZIF-8 after thermal treatment, in the presence of chaotropic agent (urea), in the presence of proteolytic agent (4 mg mL-1 protease, 2 h) or after exposure to organic solvent (DMSO or THF, 2h). (b) Cycling runs for the degradation of 0.15 mM $H_2O_2$ in the presence of 40 nM (based on FCAT) FCAT@MAF-7 at room temperature.

Encouraged by the excellent stability of FCAT@MAF-7, we sought to investigate recyclability, a critical performance metric for practical applications. We cycled FCAT@MAF-7 ten times without an appreciable reduction in enzymatic activity (Figure 4b). Furthermore, fluorescence spectroscopy confirmed negligible leaching during repeated usage. (Figure S33) and PXRD analysis showed that crystallinity was retained subsequent to the cycling process (Figure S34). Lastly, we explored the generality of MAF-7 as a host for biomacromolecules by performing an analogous set of experiments on fluorescein-tagged urease, FU. After immobilization, FU@MAF-7 retained 82% of the urease activity compared with FU@ZIF-90 (21%) and FU@ZIF-8 (13%) (Figure S43). In addition, compared with ZIF-90 and ZIF-8, MAF-7 provided better protection: FU@MAF-7 maintained 61% of

its original activity after heating (70 °C for 1h) and 74% after exposure to a proteolytic enzyme (Figure S44).

## CONCLUSION

Herein we highlight the importance of the chemistry of the ZIF and at the ZIF/biointerface for facilitating and preserving the biological function of an encapsulated enzyme. Our data show that enzymes encapsulated within MAF-7 retain a significant degree of enzymatic activity. In contrast, topologically identical ZIF-8 essentially deactivates CAT upon encapsulation or surface adsorption. Recent reports posit that optimizing hydrophobic/philic interactions between enzymes and polymers is essential for the effective encapsulation and stabilization of biomolecules.[40] Given their modular synthesis, porosity and chemical and structural diversity MOFs represent a new class of materials poised for further exploration in the area of biomolecule protection.

## ASSOCIATED CONTENT

**Supporting Information**.
Information related to synthesis, additional experimental and analytical detail. This material is available free of charge via the Internet at http://pubs.acs.org.

## AUTHOR INFORMATION

**Corresponding Author**

*Email: christian.doonan@adelaide.edu.au; paolo.falcaro@tugraz.at; christopher.sumby@adelaide.edu.au

**Author Contributions**

All authors have given approval to the final version of the manuscript.

**Funding Sources**

Australian Research Council Discovery Project (DP170103531) and National Natural Science Foundation of China (21571037).

**Notes**

The authors declare no competing financial interest.

## ACKNOWLEDGMENT

This work was supported by the Australian Research Council under the Discovery Projects Scheme (DP170103531). N. K. Maddigan acknowledges an Australian Government Research Training Program Scholarship. The authors acknowledge the facilities, and the scientific and technical assistance of the Australian Microscopy & Microanalysis Research Facility at the Adelaide Microscopy Unit, The University of Adelaide. This work used resources and services from the National Computational Infrastructure. We acknowledge the CERIC-ERIC consortium for the access to experimental facility and financial support, under proposal N 20182161. We acknowledge Elettra - Sincrotrone Trieste for provision of synchrotron radiation facilities (proposal N. 20175225). Miriam Zappatore and Nicola Cefari are acknowledged for help during the FTIR measurements/interpretations. Raffaele Ricco' is acknowledged for help during the experiments. P.F. acknowledges TU Graz for the Lead Project (LP-03).

## REFERENCES

1. Furukawa, H.; Cordova, K. E.; O'Keeffe, M.; Yaghi, O. M.,*The Chemistry and Applications of Metal-Organic Frameworks*. *Science* **2013,** 341, (6149).
2. Chen, W.-H.; Vázquez-González, M.; Zoabi, A.; Abu-Reziq, R.; Willner, I.,*Biocatalytic cascades driven by enzymes encapsulated in metal–organic framework nanoparticles*. *Nat. Catal.* **2018,** 1, 689-695.
3. Liang, K.; Ricco, R.; Doherty, C. M.; Styles, M. J.; Bell, S.; Kirby, N.; Mudie, S.; Haylock, D.; Hill, A. J.; Doonan, C. J.; Falcaro, P.,*Biomimetic mineralization of metal-organic frameworks as protective coatings for biomacromolecules*. *Nat. Commun.* **2015,** 6, 7240.
4. Liao, F.-S.; Lo, W.-S.; Hsu, Y.-S.; Wu, C.-C.; Wang, S.-C.; Shieh, F.-K.; Morabito, J. V.; Chou, L.-Y.; Wu, K. C. W.; Tsung, C.-K.,*Shielding against Unfolding by Embedding Enzymes in Metal–Organic Frameworks via a de Novo Approach*. *J. Am. Chem. Soc.* **2017,** 139, (19), 6530-6533.
5. Shieh, F.-K.; Wang, S.-C.; Yen, C.-I.; Wu, C.-C.; Dutta, S.; Chou, L.-Y.; Morabito, J. V.; Hu, P.; Hsu, M.-H.; Wu, K. C. W.; Tsung, C.-K.,*Imparting Functionality to Biocatalysts via Embedding Enzymes into Nanoporous Materials by a de Novo Approach: Size-Selective Sheltering of Catalase in Metal–Organic Framework Microcrystals*. *J. Am. Chem. Soc.* **2015,** 137, (13), 4276-4279.
6. Liang, W.; Ricco, R.; Maddigan, N. K.; Dickinson, R. P.; Xu, H.; Li, Q.; Sumby, C. J.; Bell, S. G.; Falcaro, P.; Doonan, C. J.,*Control of Structure Topology and Spatial Distribution of Biomacromolecules in Protein@ZIF-8 Biocomposites*. *Chem. Mater.* **2018,** 30, (3), 1069-1077.
7. Doonan, C.; Riccò, R.; Liang, K.; Bradshaw, D.; Falcaro, P.,*Metal–Organic Frameworks at the Biointerface: Synthetic Strategies and Applications*. *Acc. Chem. Res.* **2017,** 50, (6), 1423-1432.
8. Liang, K.; Coghlan, C. J.; Bell, S. G.; Doonan, C.; Falcaro, P.,*Enzyme encapsulation in zeolitic imidazolate frameworks: a comparison between controlled co-precipitation and biomimetic mineralisation*. *Chem. Commun.* **2016,** 52, (3), 473-476.
9. Li, S.; Dharmarwardana, M.; Welch, R. P.; Benjamin, C. E.; Shamir, A. M.; Nielsen, S. O.; Gassensmith, J. J.,*Investigation of Controlled Growth of Metal–Organic Frameworks on Anisotropic Virus Particles*. *ACS Appl. Mater. Interfaces* **2018,** 10, (21), 18161-18169.
10. Li, S.; Dharmarwardana, M.; Welch, R. P.; Ren, Y.; Thompson, C. M.; Smaldone, R. A.; Gassensmith, J. J.,*Template-Directed Synthesis of Porous and Protective Core–Shell Bionanoparticles*. *Angew. Chem., Int. Ed.* **2016,** 55, (36), 10691-10696.
11. Liang, K.; Richardson, J. J.; Doonan, C. J.; Mulet, X.; Ju, Y.; Cui, J.; Caruso, F.; Falcaro, P.,*An Enzyme-Coated Metal–Organic Framework Shell for Synthetically Adaptive Cell Survival*. *Angew. Chem., Int. Ed.* **2017,** 56, (29), 8510-8515.
12. Riccò, R.; Liang, W.; Li, S.; Gassensmith, J. J.; Caruso, F.; Doonan, C.; Falcaro, P.,*Metal–Organic Frameworks for Cell and Virus Biology: A Perspective*. *ACS Nano* **2018,** 12, (1), 13-23.
13. Garcia, C.; Junior, I. I.; de Souza, R. O. M. A.; Luque, R.,*Novel nanoparticle/enzyme biosilicified nanohybrids for advanced heterogeneously catalyzed protocols*. *Catal. Sci. Technol.* **2015,** 5, (3), 1840-1846.
14. Itabaiana, I.; Sutili, F. K.; Leite, S. G. F.; Gonçalves, K. M.; Cordeiro, Y.; Leal, I. C. R.; Miranda, L. S. M.; Ojeda, M.; Luque, R.; de Souza, R. O. M. A.,*Continuous flow valorization of fatty acid waste using silica-immobilized lipases*. *Green Chem.* **2013,** 15, (2), 518-524.

15. Park, K. S.; Ni, Z.; Côté, A. P.; Choi, J. Y.; Huang, R.; Uribe-Romo, F. J.; Chae, H. K.; O'Keeffe, M.; Yaghi, O. M.,*Exceptional chemical and thermal stability of zeolitic imidazolate frameworks*. *Proc. Natl. Acad. Sci.* **2006,** 103, (27), 10186-10191.
16. Zhang, J.-P.; Zhu, A.-X.; Lin, R.-B.; Qi, X.-L.; Chen, X.-M.,*Pore Surface Tailored SOD-Type Metal-Organic Zeolites*. *Adv. Mater.* **2011,** 23, (10), 1268-1271.
17. Rabe, M.; Verdes, D.; Seeger, S.,*Understanding protein adsorption phenomena at solid surfaces*. *Adv. Colloid Interface Sci.* **2011,** 162, (1), 87-106.
18. Zoungrana, T.; Findenegg, G. H.; Norde, W.,*Structure, Stability, and Activity of Adsorbed Enzymes*. *J. Colloid Interface Sci.* **1997,** 190, (2), 437-448.
19. Morris, W.; Doonan, C. J.; Furukawa, H.; Banerjee, R.; Yaghi, O. M.,*Crystals as Molecules: Postsynthesis Covalent Functionalization of Zeolitic Imidazolate Frameworks*. *J. Am. Chem. Soc.* **2008,** 130, (38), 12626-12627.
20. Ortiz, A. U.; Freitas, A. P.; Boutin, A.; Fuchs, A. H.; Coudert, F.-X.,*What makes zeolitic imidazolate frameworks hydrophobic or hydrophilic? The impact of geometry and functionalization on water adsorption*. *Phys. Chem. Chem. Phys.* **2014,** 16, (21), 9940-9949.
21. Ou, P.; Wolff, S. P.,*A discontinuous method for catalase determination at 'near physiological' concentrations of H2O2 and its application to the study of H2O2 fluxes within cells*. *J. Biochem. Biophys. Methods* **1996,** 31, (1), 59-67.
22. Fita, I.; Rossmann, M. G.,*The NADPH binding site on beef liver catalase*. *Proc. Natl. Acad. Sci.* **1985,** 82, (6), 1604-1608.
23. Vilanova, O.; Mittag, J. J.; Kelly, P. M.; Milani, S.; Dawson, K. A.; Rädler, J. O.; Franzese, G.,*Understanding the Kinetics of Protein–Nanoparticle Corona Formation*. *ACS Nano* **2016,** 10, (12), 10842-10850.
24. Zaak, H.; Siar, E.-H.; Kornecki, J. F.; Fernandez-Lopez, L.; Pedrero, S. G.; Virgen-Ortíz, J. J.; Fernandez-Lafuente, R.,*Effect of immobilization rate and enzyme crowding on enzyme stability under different conditions. The case of lipase from Thermomyces lanuginosus immobilized on octyl agarose beads*. *Process Biochem.* **2017,** 56, 117-123.
25. Li, Y.; Ogorzalek, T. L.; Wei, S.; Zhang, X.; Yang, P.; Jasensky, J.; Brooks, C. L.; Marsh, E. N. G.; Chen, Z.,*Effect of immobilization site on the orientation and activity of surface-tethered enzymes*. *Phys. Chem. Chem. Phys.* **2018,** 20, (2), 1021-1029.
26. Schroeder, M. M.; Wang, Q.; Badieyan, S.; Chen, Z.; Marsh, E. N. G.,*Effect of Surface Crowding and Surface Hydrophilicity on the Activity, Stability and Molecular Orientation of a Covalently Tethered Enzyme*. *Langmuir* **2017,** 33, (28), 7152-7159.
27. Cui, J.; Feng, Y.; Jia, S.,*Silica encapsulated catalase@metal-organic framework composite: A highly stable and recyclable biocatalyst*. *Chem. Eng. J.* **2018,** 351, 506-514.
28. Cui, J.; Feng, Y.; Lin, T.; Tan, Z.; Zhong, C.; Jia, S.,*Mesoporous Metal–Organic Framework with Well-Defined Cruciate Flower-Like Morphology for Enzyme Immobilization*. *ACS Appl. Mater. Interfaces* **2017,** 9, (12), 10587-10594.
29. Du, Y.; Gao, J.; Liu, H.; Zhou, L.; Ma, L.; He, Y.; Huang, Z.; Jiang, Y.,*Enzyme@silica nanoflower@metal-organic framework hybrids: A novel type of integrated nanobiocatalysts with improved stability*. *Nano Research* **2018,** 11, (8), 4380-4389.
30. Beers, R. F.; Sizer, I. W.,*Progressive inhibition of the catalase-hydrogen peroxide system by acetate, chloride and azide*. *Arch. Biochem. Biophys.* **1956,** 60, (1), 115-125.
31. Dong, X.; Fan, Y.; Yang, P.; Kong, J.; Li, D.; Miao, J.; Hua, S.; Hu, C.,*Ultraviolet-visible (UV-Vis) and fluorescence spectroscopic investigation of the interactions of ionic liquids and catalase*. *Appl. Spectrosc.* **2016,** 70, (11), 1851-1860.
32. Vivian, J. T.; Callis, P. R.,*Mechanisms of Tryptophan Fluorescence Shifts in Proteins*. *Biophys. J.* **2001,** 80, (5), 2093-2109.
33. Barth, A.,*Infrared spectroscopy of proteins*. *Biochim. Biophys. Acta Bioenerg.* **2007,** 1767, (9), 1073-1101.
34. Jackson, M.; Mantsch, H. H.,*The Use and Misuse of FTIR Spectroscopy in the Determination of Protein Structure*. *Crit. Rev. Biochem. Mol. Biol.* **1995,** 30, (2), 95-120.
35. Maté, M. J.; Zamocky, M.; Nykyri, L. M.; Herzog, C.; Alzari, P. M.; Betzel, C.; Koller, F.; Fita, I.,*Structure of catalase-A from Saccharomyces cerevisiae11Edited by R. Huber*. *J. Mol. Biol.* **1999,** 286, (1), 135-149.
36. Shivu, B.; Seshadri, S.; Li, J.; Oberg, K. A.; Uversky, V. N.; Fink, A. L.,*Distinct β-Sheet Structure in Protein Aggregates Determined by ATR–FTIR Spectroscopy*. *Biochemistry* **2013,** 52, (31), 5176-5183.
37. Zandomeneghi, G.; Krebs, M. R. H.; McCammon, M. G.; Fändrich, M.,*FTIR reveals structural differences between native β-sheet proteins and amyloid fibrils*. *Protein Sci.* **2004,** 13, (12), 3314-3321.
38. Monera, O. D.; Kay, C. M.; Hodges, R. S.,*Protein denaturation with guanidine hydrochloride or urea provides a different estimate of stability depending on the contributions of electrostatic interactions*. *Protein Sci.* **1994,** 3, (11), 1984-1991.
39. Sheldon, R. A.; Woodley, J. M.,*Role of Biocatalysis in Sustainable Chemistry*. *Chem. Rev.* **2018,** 118, (2), 801-838.
40. Panganiban, B.; Qiao, B.; Jiang, T.; DelRe, C.; Obadia, M. M.; Nguyen, T. D.; Smith, A. A. A.; Hall, A.; Sit, I.; Crosby, M. G.; Dennis, P. B.; Drockenmuller, E.; Olvera de la Cruz, M.; Xu, T.,*Random heteropolymers preserve protein function in foreign environments*. *Science* **2018,** 359, (6381), 1239-1243.

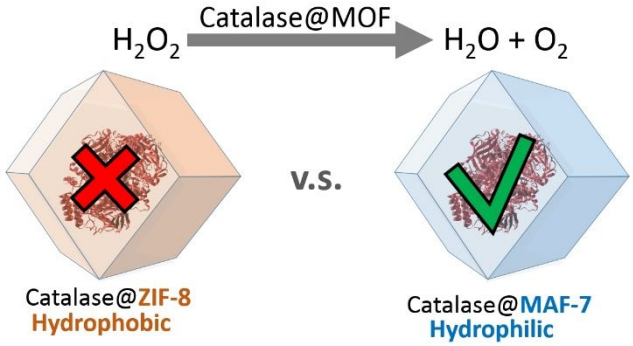
$H_2O_2$
Catalase@MOF
$H_2O + O_2$
v.s.
Catalase@ZIF-8
Hydrophobic
Catalase@MAF-7
Hydrophilic